PAPER

Check for updates

Sustainable green synthesis of *Hedychium coronarium* leaf extract-stabilized silver nanoparticles and their applications: colorimetric sensing of Sn²⁺ and Hg²⁺ and antifungal and antimicrobial properties†

Sanjay Kumar Sahu, [ID] [a] Anjana Kushwaha,[a] Umakant Pradhan,[b] Purusottam Majhi,[b] Awadesh Kumar Shukla*[b] and Tanmay Kumar Ghorai [ID] *[a]

Hedychium coronarium (Hc) (commonly known as Gulbakawali) leaf extract was used for the stable and sustainable green synthesis of silver nanoparticles (Hc-AgNPs), which were biodegradable and non-toxic. *Hedychium coronarium* leaf extract was used as a reducing agent to stabilize the Hc-AgNPs by converting Ag^+ to Ag^0 without adding any capping agent. It demonstrated stability for up to six months, and no agglomeration was observed. The Hc-AgNPs were characterized using X-ray diffraction (XRD), Fourier-transform infrared spectroscopy (FT-IR), transmission electron microscopy (TEM), ultraviolet-visible spectrophotometry, and fluorescence spectroscopy analysis. The UV-visible spectrum supported the formation of stable Hc-AgNPs by displaying a strong surface plasmon resonance (SPR) peak at 440 nm. FT-IR spectra showed the functional groups present in the leaf extract of *Hedychium coronarium*, which was the primary source of secondary metabolites attached to Ag^0. XRD analysis revealed a distinct 2θ peak of Hc-AgNPs at 38.15°, indicating a face-centred cubic structure with a crystallite size of 22.6 ± 1 nm at the (111) plane. Moreover, TEM demonstrated the spherical morphology of the Hc-AgNPs with an average particle size of 22.42 ± 1 nm. The photophysical characteristics of the Hc-AgNPs, as highlighted by their UV-vis and fluorescence characteristics, revealed their semiconducting nature with an impressive band gap (E_g) value of 3.78 eV. Fascinatingly, the fluorescence activity of Hc-AgNPs at 504 nm showed a broad emission band corresponding to the absorption band at 251 nm. We performed the selective colorimetric sensing of Sn^{2+} metal ions using Hc-AgNPs, which demonstrated a detection limit of 10^{-3} M, suggesting their potential as very good solid biosensors. Interestingly, the Hc-AgNPs showed antifungal activity, which has not been reported before. Specifically, the results showed that the Hc-AgNPs had a higher fungitoxicity effect against *Aspergillus flavus* (59.58 ± 3.68) than against *Fusarium oxysporum* (57.93 ± 4.18). The antibacterial activity of the Hc-AgNPs was evaluated against three Gram-negative phytopathogenic bacteria: *Xanthomonas oryzae* (*X. oryzae*), *Ralstonia solanacearum* (*R. solanacearum*), and *Erwinia carotovora* (*E. carotovora*), showing effective inhibition zones of 16.33 ± 0.57, 15.33 ± 0.57, and 14.33 ± 0.57 mm, respectively. These results indicate that the Hc-AgNPs could inhibit these phytopathogenic bacteria with varying degrees of effectiveness in the order of *X. oryzae* > *R. solanacearum* > *E. carotovora*.

1. Introduction

In recent years, the green synthesis of metal nanoparticles from aqueous plant extracts has attracted significant attention from researchers. This method has been established for its eco-friendliness, cost-effectiveness, non-toxicity, pollutant-free processes, and ability to harmlessly produce well-characterized nanoparticles or their oxides. One of the most precise methods is the production of metal nanoparticles involving living organisms. Among these living organisms, plants have emerged as the best candidates. They are

[a]*Nanomaterials and Crystal Design Laboratory, Department of Chemistry, Indira Gandhi National Tribal University, Amarkantak, 484887, Madhya Pradesh, India. E-mail: tanmay.ghorai@igntu.ac.in*

[b]*Microbiology Laboratory, Department of Botany, Indira Gandhi National Tribal University, Amarkantak, 484887, Madhya Pradesh, India. E-mail: awadesh.shukla@igntu.ac.in*

particularly suitable for the large-scale biosynthesis of nanoparticles. Nanoparticles synthesized from plant extracts demonstrate exceptional stability, are readily available, and have a faster synthesis rate than those produced using microorganisms. The synthesis of metal nanoparticles using *Hedychium coronarium* medicinal plant extract with coinage metals (Cu, Ag, and Au) is a formidable challenge. However, these nanoparticles offer potential in a diverse range of applications, including in photocatalysis; colorimetric sensing; bioimaging; surface-enhanced Raman scattering; antifungal, antimicrobial, and antioxidant applications; drug delivery; chemotherapeutics; and DNA and BSA binding.[1–17]

Nanoscience and nanotechnology are playing increasingly important roles in biological science for the biosynthesis of AgNPs using different techniques to tailor their fabrication with special physical and chemical properties for use in various applications in the medical field.[18–28] Jadhav *et al.* reported the chemotherapeutic activity of AgNPs synthesized using an aqueous extract of *Salacia Chinensis* bark.[29] Sarker and co-authors reported the use of an aqueous leaf extract of *Caesalpinia digyna* as a reducing and capping agent for the size- and shape-controlled fabrication of AgNPs and investigated their antimicrobial activity.[30] Das *et al.* reported the pH-controlled synthesis of AgNPs using an aqueous bark extract of *Butea monosperma* (Lam.) Taub., showcasing its remarkable efficiency in nanoparticle formation.[31] Mutairi *et al.* presented the green synthesis of AgNPs and accessed their antifungal and antibacterial properties using *Phoenix dactylifera* L. leaf extract (Saudi Palm Tree).[32] Haibing Yu and co-workers reported the synthesis of AgNPs utilizing *Ligustrum lucidum* leaf extract, and explored its innovative role in nanoparticle formation and then investigated its antifungal potential.[33]

Water pollution is becoming an increasingly significant problem nowadays due to the presence of heavy metal ions in water, like Li^+, Ca^{2+}, Fe^{3+}, Ni^{2+}, Hg^{2+}, Cd^{2+}, Sn^{2+}, Zn^{2+}, Mn^{2+}, Cu^{2+}, Na^+, and Mg^{2+}, leading to metal toxicity of the water. These are some essential metals that are needed for maintaining life, but their misbalance, even at the ppm level concentration, can lead to various issues, such as growth disorders, severe malfunction, carcinogenesis, or even death. Therefore, the sensing of toxic metals in the aquatic environment and biological system has received much attention with demands for rapid and cost-efficient approaches to protect the health and safety of the public and ecosystems. Several recent reports have focused on discerning heavy metal cations using numerous analytical instruments.[19,34–36] Mercury is a ubiquitous, stable neurotoxic element that is responsible for the peroxidation of lipids, and for mitochondrial and microtubule destruction. Exposure to toxic mercury can lead to behavioural and neurological changes in animals.[37] Various industrial activities are the primary sources of mercury pollution in the environment, such as the paper, pharmaceuticals, power plants, agriculture, caustic soda and chlorine, laboratories, and fuel-refining industries.[38,39] Besides mercury, organotin compounds are raising concerns. However, the toxicity levels of organotin compounds vary significantly, with most considered either nontoxic or exhibiting low-level toxicity, while others are deemed highly toxic. The molecular structure plays a crucial role in determining the toxicity level of these compounds.

The white garland lily, also known as the white ginger lily or *Hedychium coronarium*, is a perennial flowering plant in the Zingiberaceae family. It is a rhizomatous herb widely used in Indian Ayurvedic medicines as a febrifuge, eye tonic, anti-rheumatic, anthelmintic, and mild tranquillizer. The main threats to this plant are over-exploitation of its rhizome for medicinal purposes and the resulting destruction of its natural habitat. This work presents the novel synthesis of a silver nanoparticles complex (Hc-AgNPs) using *Hedychium coronarium* leaf extract, and then a thoroughly examination of the antifungal and antibacterial properties of the complex and its potential application in sensing metal cations. This innovative approach has not been previously reported. *Hedychium coronarium* is rich in secondary metabolites, such as alkaloids, phenols, flavonoids, terpenoids, steroids, and glycosides, and thus can serve as an excellent source material for synthesizing Hc-AgNPs in an aqueous medium. Our study successfully demonstrated the effective sensing of specific metal ions and the potent antifungal and antimicrobial activity of the Hc-AgNPs.

2.   Experimental section

2.1.   Material and methods

2.1.1.   Plant material. Fresh and healthy leaves of *Hedychium coronarium*, also known as Gulbakawali (Fig. 1), were harvested at the IGNTU campus herbal garden in Amarkantak, Anuppur, Madhya Pradesh. Experts in the field verified the identity of the plant species. To verify the authenticity, a voucher specimen bearing the label "voucher specimen IGNTU/DOB/2023/Zin/HC/12" was meticulously recorded and placed in the Chemistry Department of the Indira Gandhi National Tribal University, Amarkantak, Madhya Pradesh, India.

Fig. 1 *Hedychium coronarium* plant with flowers.

Table 1   Phytochemical analysis of HCLE

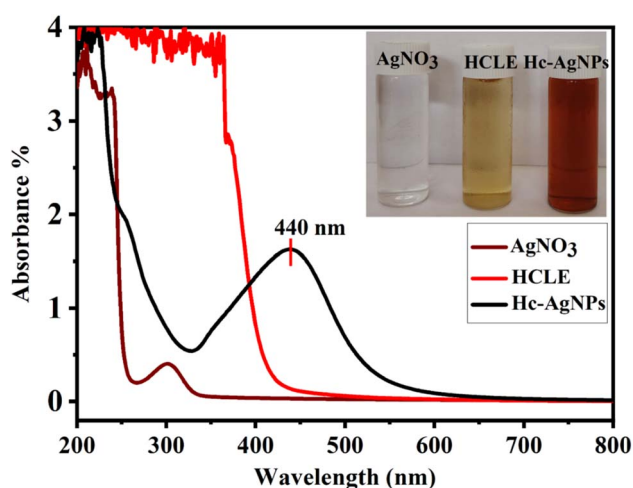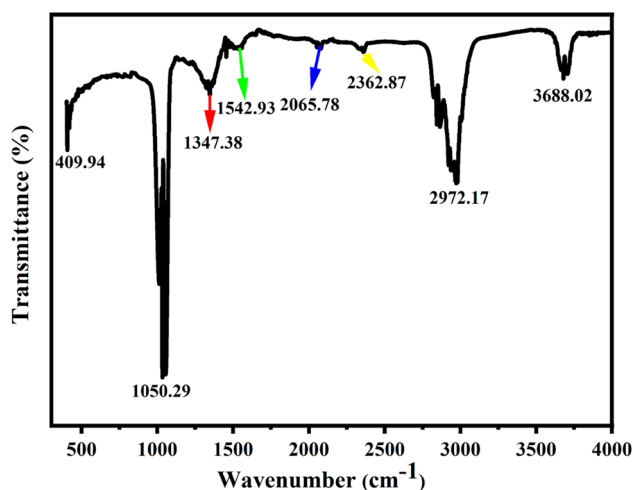| SI. no.	Phytochemicals	Phytochemical test performed	Observation	Results	References
1	Flavonoids	Ferric chloride test	Blackish precipitate appeared	+ve	41
		Basic lead acetate test	Yellow precipitate appeared	+ve	42
2	Diterpenes	Copper acetate test	Green colour appeared	+ve	41
3	Triterpenes	Salkowski test	The lower phase later turned yellow	+ve	41
4	Steroids	Salkowski test	No changes observed	−ve	41
5	Cardiac glycoside	Keller–Kiliani test	Bluish brown ring observed at junction of two layers	+ve	41 and 43
6	Alkaloids	Hager's test	Yellow precipitate appeared	+ve	42
		Wagner's test	Reddish-brown precipitate	+ve	41 and 42
7	Phenols	10% ferric chloride test	Formation of green colour	+ve	41

Fig. 2   UV-Vis spectra of Hc-AgNPs.

Fig. 3   FT-IR spectrum of the Hc-AgNPs.

2.1.2. Chemicals. The chemicals listed in the following were purchased from Himedia (AR Grade) and used in the experiments as received without any further purification. The chemicals included silver nitrate ($AgNO_3$), ferric chloride ($FeCl_3$), copper chloride dihydrate ($CuCl_2 \cdot 2H_2O$), manganese chloride ($MnCl_2$), lithium chloride (LiCl), mercuric chloride ($HgCl_2$), cadmium chloride ($CdCl_2$), calcium chloride ($CaCl_2$), stannus chloride ($SnCl_2$), nickel chloride ($NiCl_2$), sodium chloride (NaCl), manganese chloride hexahydrate ($MgCl_2 \cdot 6H_2O$), zinc chloride ($ZnCl_2$), lead acetate [$Pb(CH_3COOH)_2$], iodine (I_2), potassium iodide (KI), chloroform ($CHCl_3$), conc. sulfuric acid (H_2SO_4), acetic acid (CH_3COOH), and copper acetate [$Cu(CH_3COOH)_2$], dimethyl sulfoxide (DMSO), potato dextrose agar (PDA), Mueller–Hinton agar (MHA), and ciprofloxacin.

2.2. Preparation of the leaf extract

The leaves of *Hedychium coronarium* were collected fresh and in good condition, and they were thoroughly cleaned using tap water and then deionized water. This process aimed to remove any dirt, contaminants, or impurities. After that, the leaves were chopped into small pieces and left to dry for three days in the shade. For extraction, 3 g of the sliced leaves and 100 mL of water were added to a 250 mL beaker. Subsequently, the mixture was heated for about 45 min at approximately 70–80 °C to facilitate the swift release and dispersion of phytochemicals within the solution, and then left to cool for half an hour. Upon filtration, the leaf extract was stored in the refrigerator at 4 °C for later use.

2.3 Phytochemical analysis

A preliminary qualitative phytochemical analysis was carried out using the following standard procedure described below to identify and record the essential components of the phytochemicals contained in the HCLE (*Hedychium coronarium* leaf extract).[40] Table 1 presents the findings of this analysis.
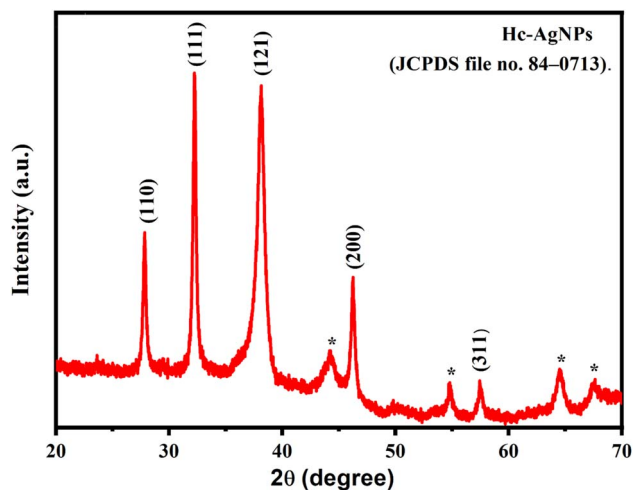
2.4. Green synthesis of Hc-AgNPs

Silver nitrate (0.0305 g, 5 mM) was dissolved in 36 mL distilled water in a 100 mL beaker and stirred for about 10 min. Then, 4 mL of the aqueous *Hedychium coronarium* leaf extract was added to the solution. The reaction mixture was continuously stirred at a steady 450 rpm and maintained at room temperature for an optimal duration of 150 min. Within 5 min, the initial colour of the solution changed from light green to reddish-brown, as observed visually and as confirmed by UV-vis spectroscopy measurement through the surface plasmon resonance (SPR) band indicating the formation of Hc-AgNPs. The

Table 2 FT-IR spectral data of the Hc-AgNPs and corresponding stretching frequencies of the functional group present in the composites

Hc-AgNPs wavenumber	Probable functional group	Hc-AgNPs wavenumber	Probable functional group
409.94	Metal oxide or metal nitrite	2065.78	C≡C stretching
1050.29	C–N stretching	2362.87	C–H stretching of a methylene group
1347.38	O–H bending	2972.17	C–H (vinyl)
1542.93	O–C stretching	3688.02	O–H free

Fig. 4 XRD pattern of the Hc-AgNPs.

reaction mixture was left in the dark overnight to ensure that AgNO$_3$ was reduced entirely and its spectrum was rechecked. Finally, the reaction mixture was centrifuged for 10 min at 10 500 rpm to settle the nanoparticles. After that, the mixture's upper layer was decanted, filtered through Whatman 42 filter paper, and washed with a water and ethanol (1 : 1) mixture. Then, the nanoparticles were dried for 3–4 hours in a hot air oven and then preserved for further examination.

2.5 Characterization of the Hc-AgNPs

The reaction mixture was analyzed by UV-visible spectroscopy (UV-1800, SHIMADZU) over a scanning range of 190–900 nm to confirm the bio-reduction of AgNO$_3$ to Hc-AgNPs and evidence of the metal ions for sensing. FT-IR spectroscopy (Thermo Scientific iDZ7 ATR, Nicolet iS5) was employed to detect the functional groups in the *Hedychium coronarium* leaf extract and Hc-AgNPs. Powder X-ray diffraction (PANalytical X pert^3) was used to obtain the diffraction patterns of Hc-AgNPs with Cu Kα radiation ($\lambda = 1.5406$ Å) between 20° to 80° at room temperature. HR-TEM (HR-TEM: Jeol/JEM 2100) was performed to reveal the morphology of the Hc-AgNPs. Moreover, the materials' photoluminescence was measured at room temperature using a fluorescence spectrophotometer (PerkinElmer FL 6500).

2.6. Colorimetric metal-ions-recognition ability of the Hc-AgNPs

The colorimetric detection capacity of the Hc-AgNPs was evaluated by testing a variety of metal cations, *i.e.*, Li$^+$, Ca^{2+}, Fe^{3+},

Ni^{2+}, Hg^{2+}, Cd^{2+}, Sn^{2+}, Zn^{2+}, Mn^{2+}, Cu^{2+}, Na$^+$, and Mg^{2+}. The colorimetric sensing methodology followed that set out by Annadhasan *et al.* (2014).[1] We prepared aqueous solutions of 10^{-3} M of each metal salt (LiCl, CaCl$_2$, FeCl$_3$, NiCl$_2$, HgCl$_2$, CdCl$_2$, SnCl$_2$, ZnCl$_2$, MnCl$_2$, CuCl$_2$·2H$_2$O, NiCl$_2$, NaCl, and MgCl$_2$·6H$_2$O) for analyzing the sensing properties of the Hc-AgNPs. Equal volumes of the Hc-AgNPs solution and 1000 μL of the aqueous metal salt solution were added in to experimental vials. Among all the metal ions selectively tested, only Sn^{2+} and Hg^{2+} changed colour from reddish-brown to deep-brown and colourless in the presence of Hc-AgNPs, respectively.

2.7. Study of the antifungal activity of Hc-AgNPs using the food poisoning method

In vitro antifungal activity studies of the Hc-AgNPs were conducted against two phytopathogenic fungi, *Fusarium oxysporum* and *Aspergillus flavus*, using the food poisoning method. These two fungi were obtained from the National Culture Collection of Pathogenic Fungi (NCCPF), Department of Medical Microbiology, Chandigarh, India. To assess the fungitoxicity effect of Hc-AgNPs, three different concentrations (0.5, 1, and 1.5 mg mL^{-1}) were made by dissolving them in 5% dimethyl sulfoxide (DMSO), then mixing them separately in 9 mm presterilized Petri plates containing 20 mL of sterilized molten potato dextrose agar (PDA), and then allowing the mixtures to solidify for about 5–8 min. To examine the impact on mycelial growth of two fungi, *F. oxysporum* and *A. flavus*, a 5 mm disc of a seven-day-old culture was cut out with the help of a pre-sterilized 5 mm cork borer from the periphery region and placed aseptically at the centre of each Petri plate. In the control set, only 5% DMSO was used to determine the actual effect of the Hc-AgNPs. All the Petri plates were incubated at 26 ± 2 °C in a BOD incubator for 8 days. Each treatment was carried out in triplicate. The radial mycelial growth of the tested fungi was recorded in millimetres (mm) for eight days. The percentage inhibition of the radial growth was evaluated using the following formula:

$$\text{Percentage inhibition of mycelial growth} = \frac{dc - dt}{dc} \times 100 \quad (1)$$

where dc is the fungi radial growth in the control plate (5% DMSO), and dt is the fungi radial growth in the treated plate (Hc-AgNPs + 5% DMSO).

2.8. Study of the antibacterial activity of Hc-AgNPs by the agar well diffusion method

Tested bacterial isolates were procured from Indian Type Culture Collection Identification/Culture supply Services
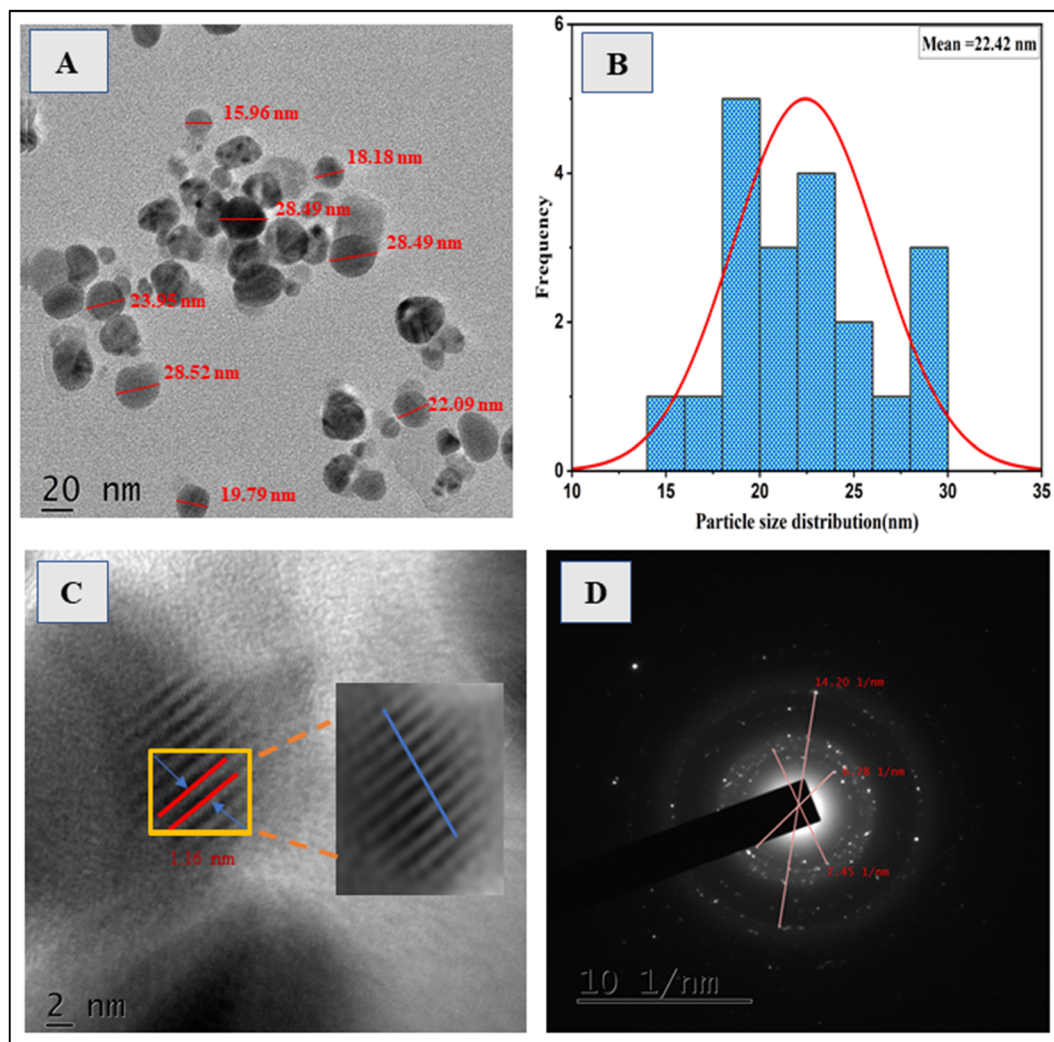
Fig. 5   (A) HR-TEM image of the Hc-AgNPs, (B) histogram plot of the Hc-AgNPs from figure (A), (C) lattice fringes at higher resolution of the Hc-AgNPs, and (D) SAED pattern of the Hc-AgNPs.

Division of Plant Pathology Indian Agricultural Research Institutes New Delhi. 110012. The agar well diffusion method was used to evaluate the antibacterial activity of the green-synthesized Hc-AgNPs against three Gram-negative phytopathogenic bacteria: *Xanthomonas oryzae*, *Ralstonia solanacearum*, and *Erwinia carotovora*, respectively. In this study, nutrient broth medium was used to subculture the bacteria, which were incubated at 37 °C for 24 h in a BOD shaker incubator. Afterwards, each overnight-grown culture was taken and spread uniformly on the respective solidified Mueller–Hinton Agar (MHA) media plates. A 5 mm well was made on each plate using a sterilized cork borer. Three different concentrations (168, 336, and 504 μg) of Hc-AgNPs were loaded into the respective wells, and ciprofloxacin was used as a control. Finally, the Petri plates were incubated at 37 °C for 24 h. The antibacterial activity of the synthesized NPs was evaluated by measuring the diameter of the inhibition zone and comparing it with the control sets. The volume of bacteria was standardized to contain approximately 1.5×10^8 CFU mL^{-1} of 0.5 McFarland standard and the volume

of NPs added, such as 6 mg mL^{-1} to 28 μL/168 μg, 56 μL/336 μg, 8428 μL/504 μg.

2.9. Statistical analysis

All the tests were examined in triplicate, and statistical analysis was performed using GraphPad Prism (9.3.1). The studies include Pearson's correlation coefficient test ($P < 0.05$) and ordinary one-way ANOVA. The results are presented as the mean ± SD from triplicate sample analysis.

3.   Results and discussion

3.1. Phytochemical analysis

Aqueous extracts of medicinal plants, such as *Hedychium coronarium* leaf extract (HCLE), are treasure troves of phytobiomolecules. These natural compounds offer a safer and healthier alternative to artificial synthetic drugs. Phytochemical analysis (Table 1) of HCLE revealed a rich presence of many beneficial compounds, including flavonoids, diterpenes, triterpenes,
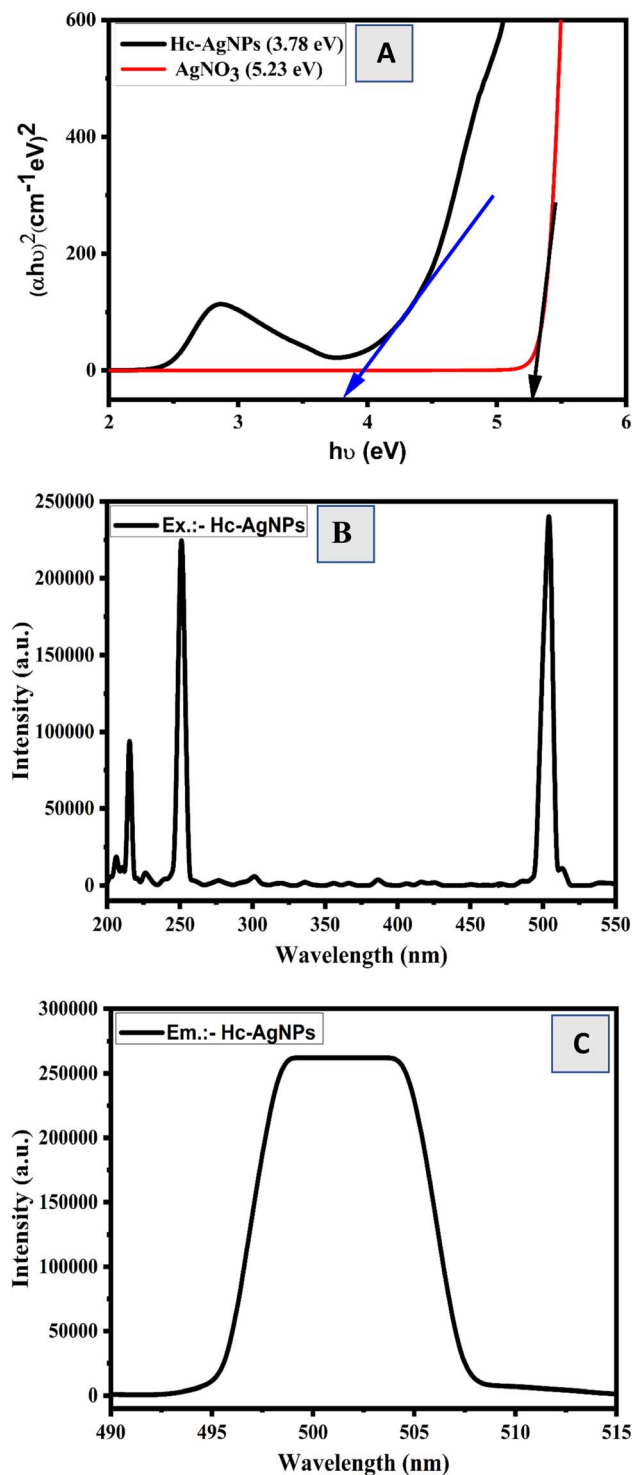
Fig. 7 UV-visible absorbance spectra of Hc-AgNPs with supplemented metal ions and the selective sensing of Sn^{2+} and Hg^{2+} metal ions by Hc-AgNPs in an aqueous medium.

3.2. UV-vis spectral analysis

The synthesis of Hc-AgNPs using aqueous *Hedychium coronarium* leaf extract was carried out under normal atmospheric conditions. Fig. 2 presents the UV-visible spectra of $AgNO_3$ solution (red-wine-coloured line), *Hedychium coronarium* leaf extract (red line), and Hc-AgNPs (black line), indicating the formation of silver nanoparticles from HCLE. The distinctive SPR band that appeared at 440 nm confirmed the formation of Hc-AgNPs, whereas no peak was detected for HCLE, and $AgNO_3$ exhibited a peak at 300 nm. These findings align with the established measurement range of SPR bands for metallic nanoparticles, which typically appear between 400–500 nm in the visible region.[44] Different researchers have also reported a similar type of SPR band for AgNPs. Susarrey-Arce *et al.* reported a 400 nm absorption spectral band for *Lysiloma acapulcensis*-mediated AgNPs.[45] N. Satsangi reported the absorption spectral band at 426.4 nm when using *Asafoetida* powder-mediated AgNPs.[46] Shaik & Adil *et al.* reported that *Origanum vulgare* leave-mediated AgNPs displayed an absorbance spectral band at 430 nm.[47] Ghannadnia *et al.* published the maximum absorption spectral band of green-synthesized AgNPs using salvia spinosa-grown extract at 450 nm.[48] Nanoparticle fabrication depends on various physicochemical factors, such as metal-ion concentration, reducing or capping agent concentration, incubation periods, pH of the reaction mixture, and temperature. Consequently, unique characteristics emerge, resulting in modifications to the nanoparticles' size, shape, yield, stability, and agglomeration of the Hc-AgNPs.

3.3. FT-IR analysis

FT-IR spectroscopy was employed to identify the various biomolecules of the leaf extract and synthesized silver nanoparticles. Fig. 3 depicts the FT-IR spectrum of the Hc-AgNPs, illustrating peaks corresponding to the functional groups found in the different phytochemicals. These functional groups, present in the Hc-AgNPs, play an essential role in both the

Fig. 6 Optical band gap and fluorescence spectra of the Hc-AgNPs. (A) Optical band gap energy of the Hc-AgNPs. (B) Excitation spectra and (C) emission spectra of the Hc-AgNPs.

cardiac glycosides, alkaloids, and phenols. Such phytobiomolecules can adsorb onto the surface of Ag^+ ions, catalyzing their reduction to Ag^0. This process not only prevents accumulation but also facilitates the synthesis of Hc-AgNPs.
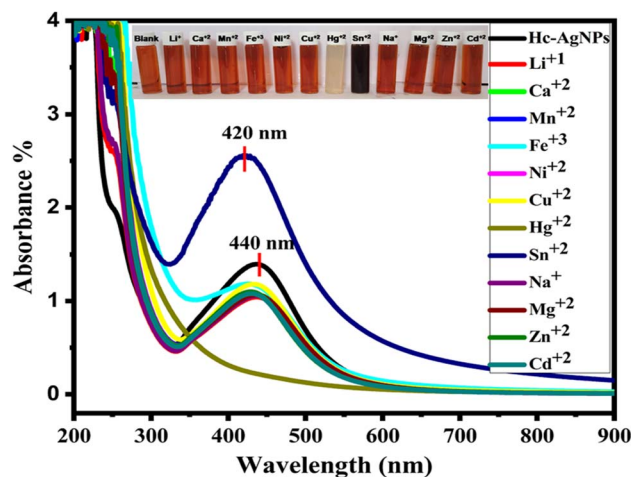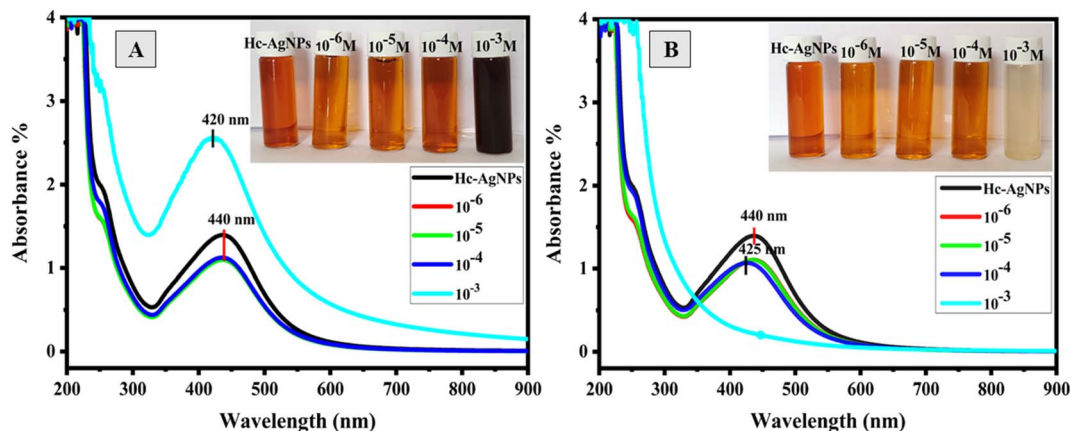
Fig. 8 UV-visible spectra of Hc-AgNPs as a function of various concentrations of (A) Sn^{2+} and (B) Hg^{2+} ions.

reduction and stabilization of the nanoparticles. Table 2 details the primary peaks observed in the FT-IR spectra, along with their respective wavenumbers and potential functional group interpretations.

3.4. XRD analysis

The lattice parameters and the crystalline nature of the green-synthesized Hc-AgNPs were assessed by XRD analysis, as shown in Fig. 4. The XRD pattern indicates the respective diffraction peak of the green-synthesized Hc-AgNPs, with 2θ values between $20°-80°$ of $27.85°$, $32.19°$, $38.19°$, $46.24°$, and $57.52°$. The corresponding (h, k, l) Miller indices values were (110), (111), (121), (200), and (311), respectively. These values match with the JCPDS file no. 84-0713 and may be indexed to the face-centred cubic structure of the Hc-AgNPs.[49] The sharp peaks shown in Fig. 4 might be due to the presence of phytochemicals, which stabilize the Hc-AgNPs, while a few unassigned peaks (*) might be related to the crystallization of the

biomolecules on the surface of the Hc-AgNPs.[40,44] Scherrer's formula, *i.e.* $D = 0.9\lambda/\beta \cos\theta$, where D is the average crystalline size (Å), λ is the X-ray radiation ($\lambda = 1.54$ Å) source, β is the singular line full width at half maximum (FWHM), and θ is Bragg's angle, was used to calculate the average crystalline size of the Hc-AgNPs as 22.6 ± 1 nm on the (111) plane.

3.5. HR-TEM analysis of the green-synthesized Hc-AgNPs

High-resolution transmission electron microscopy (HR-TEM) was performed to investigate the nanoparticles' morphology, size, and shape. Fig. 5(A) shows the HR-TEM image of the Hc-AgNPs with a spherical shape, and their average particle size was found to be 22.42 ± 1 nm as calculated by Image J software. The diameter of the nanoparticles varied from 15.96 to 28.49 nm, and are highlighted in red colour in the figure. Fig. 5(B) presents a histogram of the particle-size distribution of the Hc-AgNPs, which supported the particle-size measurements. Fig. 5(C) indicates that the lattice fringes at higher
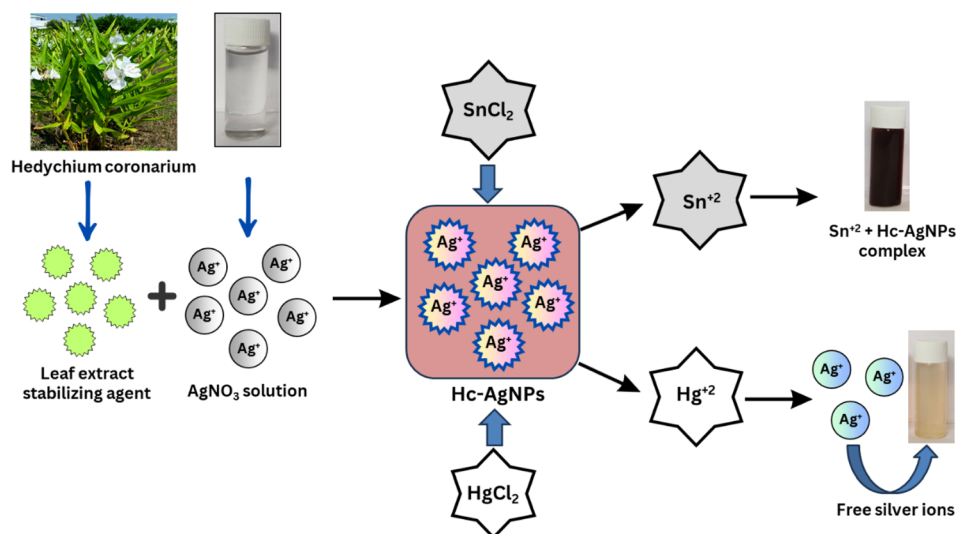

Fig. 9 Possible interaction mechanism of Hc-AgNPs with Sn^{2+} and Hg^{2+} ions.
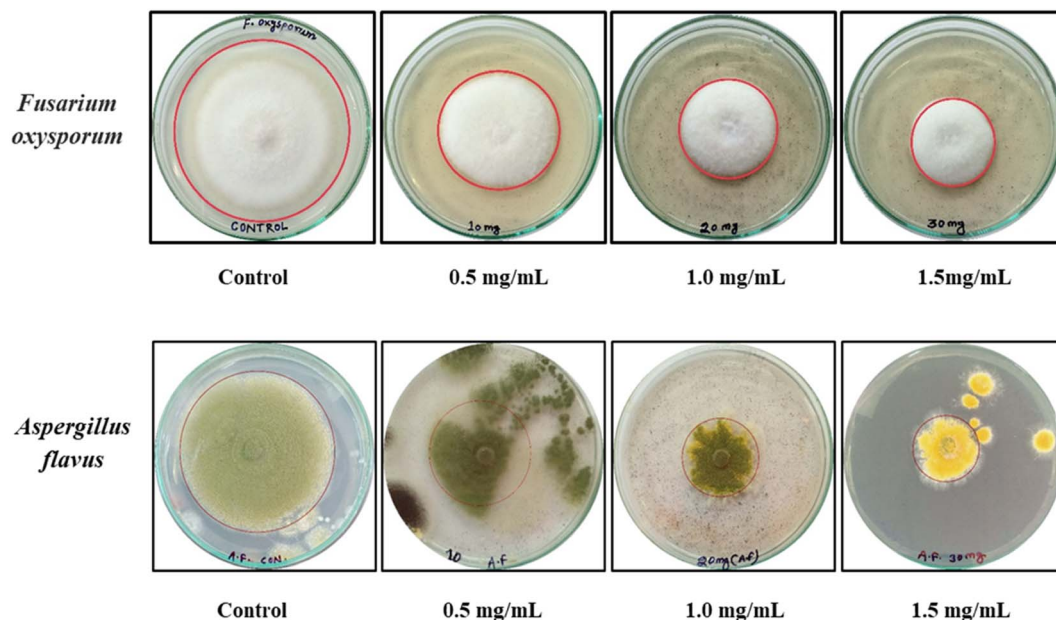
Fig. 10 Fungitoxicity effects of different concentrations of Hc-AgNPs against *Fusarium oxysporum* and *Aspergillus flavus* fungi.

resolution TEM of Hc-AgNPs have a good arrangement in the lattice. The SEAD pattern of the Hc-AgNPs proved their crystalline nature, and the corresponding (*hkl*) values assigned to the FCC lattice are shown in Fig. 5(D).

3.6. Optical properties of Hc-AgNPs

Tauc's formula eqn (2) was used to determine the conductivity and optical band gap energy of the Hc-AgNPs based on their UV spectrum. The formula is expressed as:

$$(\alpha h\nu)^n = A(h\nu - E_g) \qquad (2)$$

where the absorption coefficient is represented by α, the photon energy is indicated by $h\nu$, E_g indicates the band gap energy, A is a constant, and n is the exponent and depends on the type of transition. The band gap energy E_g of the Hc-AgNPs was calculated by plotting $(\alpha h\nu)^2$ against $h\nu$, as shown in Fig. 6(A). To do this, the linear segment of the curve had to be extrapolated to $(\alpha h\nu)^2 = 0$ and the binding energy of the materials calculated.

Fig. 6 presents the optical band gap and fluorescence spectra of Hc-AgNPs, and AgNO$_3$ for comparison.

The band gap energy corresponds to the simple moving of electrons from the valence band (BV) to the conduction band (CB). The band gap energy of Hc-AgNPs was found to be 3.78 eV, which is lower than the standard AgNO$_3$ band gap value of 5.23 eV. This indicates that the Hc-AgNPs exhibited semiconductor properties.

The fluorescence properties of Hc-AgNPs were examined using excitation and emission spectral analysis, as shown in Fig. 6(A) diluted solution of Hc-AgNPs was prepared for the experiment by dispersing 2 mg of solid Hc-AgNPs in 19 mL of ethanol and sonicating the mixture. Fig. 6(B) shows the excitation wavelengths of Hc-AgNPs, which were determined to be 251 and 504 nm, and their corresponding emission band was found at 504 nm, with a wide range, as shown in Fig. 6(C). Surprisingly, even with the excitation wavelength fixed at 251 and 504 nm, the emission spectra in both cases showed the same peak at 504 nm, suggesting that the fluorescence pattern of Hc-AgNPs was stable. The Hc-AgNPs' highest-intensity fluorescence

Table 3 Percentage inhibition (mm) of the mycelial growth of the fungi *Fusarium oxysporum* and *Aspergillus flavus* by Hc-AgNPs at different concentrations

Sl. no.	Phytopathogenic fungi	Concentration of Hc-AgNPs	Percentage inhibition of mycelial growth in (with mean ± SD)
01	*Fusarium oxysporum*	0.5 mg mL^{-1}	37.44 ± 4.27[a]
		1.0 mg mL^{-1}	48.46 ± 4.08
		1.5 mg mL^{-1}	57.93 ± 4.18
02	*Aspergillus flavus*	0.5 mg mL^{-1}	50.40 ± 4.01
		1.0 mg mL^{-1}	53.94 ± 2.52
		1.5 mg mL^{-1}	59.58 ± 3.68

[a] Each value is an average of three replicates ± standard deviation (SD).
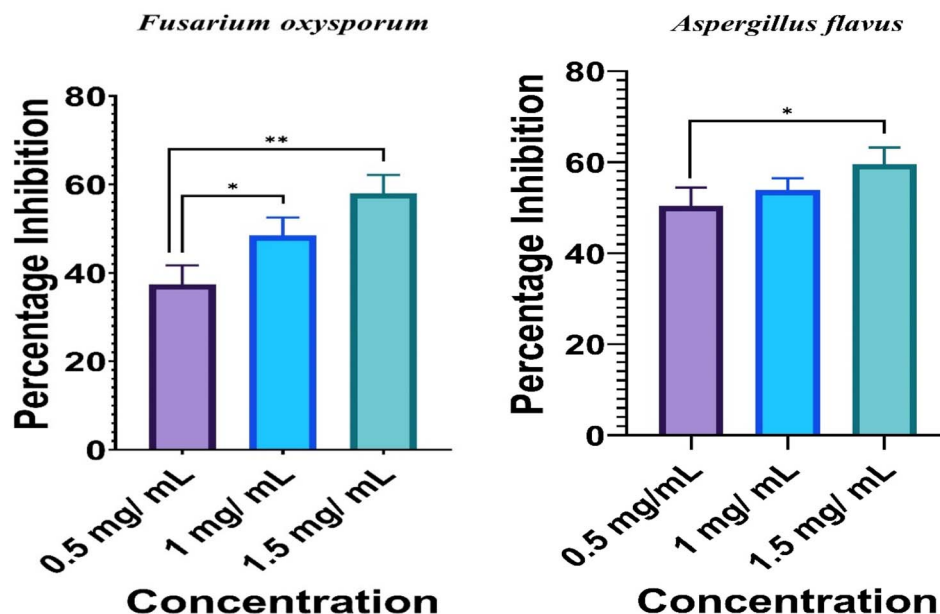
Fig. 11 Percentage inhibition of the mycelial growth of phytopathogenic fungi at different concentrations of Hc-AgNPs. The figure also presents the one-way analysis of variance (ANOVA) results. * and ** represent the significance differences between samples at $p < 0.05$ and 0.01, respectively.

spectrum show a smaller band gap, corroborating the claim that they behave well in semiconducting environments. In comparison, HCLE appeared in the excitation band at 220 nm, and its corresponding wavelength did not show any emission band, supporting that the Hc-AgNPs have a unique fluorescence behaviour.

3.7. Metal-ions-sensing ability of the Hc-AgNPs

To investigate the sensing ability of the Hc-AgNPs for various metal ions (Li^+, Ca^{2+}, Fe^{3+}, Ni^{2+}, Cd^{2+}, Hg^{2+}, Sn^{2+}, Zn^{2+}, Mn^{2+}, Cu^{2+}, Na^+, Mg^{2+} at 10^{-3} M), calorimetry was performed and the UV-visible spectra recorded. Here, 5 mM Hc-AgNPs colloidal nanoparticle solution was prepared with distilled water and

then centrifuged. Then, 3 mL of the colloidal dispersion of nanoparticles was placed in different vials, and 2 mL of a prepared 10^{-3} M heavy metal solution was added to each vial. By performing the tests, we observed prominent colour changes in Sn^{2+} from reddish-brown to deep-brown, showing the formation of a black precipitate, whereas the Hg^{2+} solution became colourless, as shown in Fig. 7. However, no change was observed in the case of the other metal systems, which indicates that they were not involved in cation–exchange reactions. From this observation, we confirmed the selective sensing of Sn^{2+} and Hg^{2+} metal ions by Hc-AgNPs in aqueous medium.

Under similar conditions, the selective detection of Sn^{2+} and Hg^{2+} ions by Hc-AgNPs was further investigated at several lower concentrations (10^{-4}, 10^{-5}, and 10^{-6} M). At these reduced

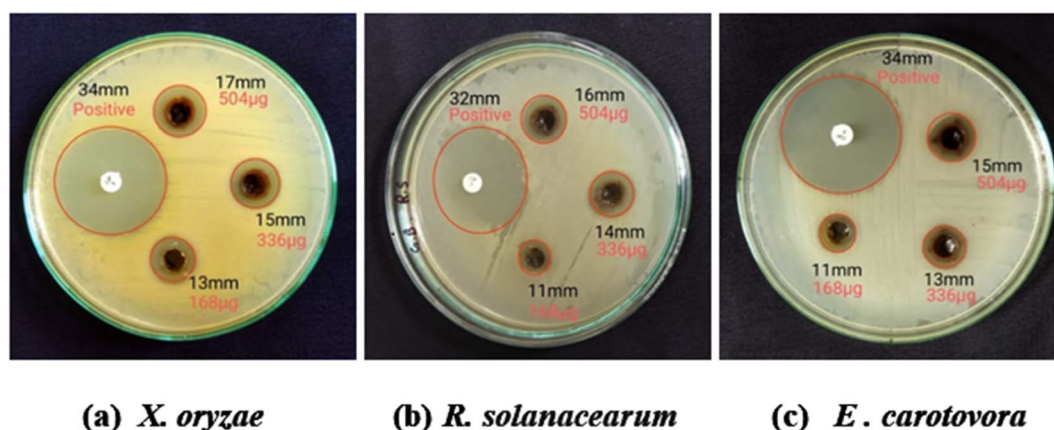(a) *X. oryzae* (b) *R. solanacearum* (c) *E . carotovora*

Fig. 12 Antibacterial activity study of different concentrations (168, 336, and 504 µg) of Hc-AgNPs against (a) *X. oryzae*, (b) *R. solanacearum*, and (c) *E. carotovora*.
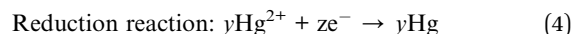
Table 4 Antibacterial activity of Hc-AgNPs at different concentrations against phytopathogenic bacteria

		Average zone of inhibition in (mm) at different concentrations of Hc-AgNPs, mean $\pm$ SD			
Sl. no	Pathogens	Positive control	168 µg	336 µg	504 µg
1	*Xanthomonas oryzae*	33.66 ± 0.57^{a}	12.00 ± 1.00	13.66 ± 1.15	16.33 ± 0.57
2	*Ralstonia solanacearum*	31.66 ± 0.57	10.33 ± 0.57	13.33 ± 0.57	15.33 ± 0.57
3	*Erwinia carotovora*	33.66 ± 0.57	10.66 ± 0.57	12.33 ± 0.57	14.33 ± 0.57

[a] Each value is an average of three replicates $\pm$ standard deviation (SD).

concentrations of both Sn^{2+} and Hg^{2+} metal ions, no discernible colour shift or modification in the UV-visible spectra was observed, as shown in Fig. 8(A) and (B). Significant changes were observed in 10^{-3} M solution of Sn^{2+} and Hg^{2+}, and their absorbance value was shifted from 440 to 420 nm (blue-shifted) and 425 nm to colourless. In the previous work, we reported the use of colorimetric sensing to detect Fe^{3+} and Hg^{2+} metal ions by SA-AgNPs.[50] Interestingly, this is the first time that the selective sensing of Sn^{2+} ions by Hc-AgNPs has been reported with *Hedychium coronarium* leaf extract containing phytochemicals and their synthesis techniques or reaction mixture. The probable mechanistic explanation for the selective sensing of metal ions (Sn^{2+} and Hg^{2+}) by Hc-AgNPs is given in Fig. 9. The adsorption intensity of Hc-AgNPs was diminished upon adding a 10^{-3} M concentration of Sn^{2+}, accompanied by a colour change from reddish-brown to deep-brown. This alteration could likely be attributed to the formation of a chelation complex on the surface of the Hc-AgNPs. The chelation complex arose from interactions between the functional groups present in the leaf extract (–OH, –COO–, and –NH$_2$) and Sn^{2+} ions. However, when Hg^{2+} metal ions (10^{-3} M) was introduced to the AgNPs, the colour shifted from brown to colourless, reducing the absorption intensity of the Hc-AgNPs. This phenomenon may be attributed to a redox reaction (eqn (5)), where the oxidation reaction (eqn (3)) involves the conversion of AgNPs to Ag^{+} ions, and the reduction reaction (eqn (4)) consists of the conversion of Hg^{2+}/Hg.

$$\text{Oxidation reaction: } x\text{Hc-AgNPs} \rightarrow x\text{Ag}^{+} + ze^{-} \quad (3)$$

$$\text{Reduction reaction: } y\text{Hg}^{2+} + ze^{-} \rightarrow y\text{Hg} \quad (4)$$

$$\text{Redox reaction reaction: } x\text{Hc-AgNPs} + y\text{Hg}^{2+} \rightarrow x\text{Ag}^{+} + y\text{Hg} \quad (5)$$

3.8. Antifungal activity studies of the Hc-AgNPs

The antifungal activity of Hc-AgNPs was examined by calculating the percentage inhibition of radial mycelial growth of tested fungi, as shown in Fig. 10. The Hc-AgNPs were found to inhibit the mycelial growth of both tested fungi. The results showed that Hc-AgNPs had a more substantial fungitoxicity effect against *A. flavus* than *F. oxysporum*. The morphological changes were observed in *A. flavus* with respect to the concentration. While increasing the concentration of NPs, the colour changed from yellow-green to caramel-mustard. This may be due to oxidative stress leading to the production of pigments. However, in the case of the fungus *F. oxysporum*, the colour change was not observed. Table 3 shows the comparative percentage inhibition of the mycelial growth of two tested fungi at different concentrations of Hc-AgNPs. At higher concentrations (1.5 mg mL^{-1}), *A. flavus* was more sensitive, with $59.58 \pm 3.68\%$ inhibition, than *F. oxysporum*, with $57.93 \pm 4.18\%$. While decreasing the concentrations to 0.5 and 1 mg mL^{-1} resulted in $37.44 \pm 4.27\%$ and $48.46 \pm 4.01\%$ inhibitions against *F. oxysporum* and $50.4 \pm 4.01\%$ and $53.94 \pm 2.52\%$ against *A. flavus*,
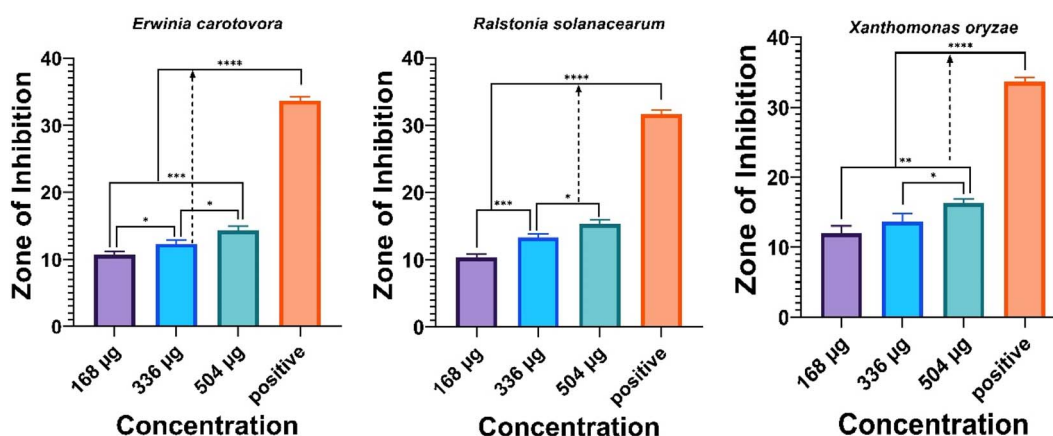

Fig. 13 Zone of inhibition of bacteria at different concentrations of Hc-AgNPs. The figure also presents the one-way analysis of variance (ANOVA) results. *, **, *** and **** represent the significance differences between samples at $p < 0.05$, 0.01, 0.001, and 0.0001, respectively.

respectively. The fungitoxicity nature of the synthesized NPs was found to be dose-dependent. Khan *et al.* (2021) reported a 40–50% reduction in the mycelial growth of *F. oxysporum* by using AgNPs, and SEM analysis confirmed the disruption of the fungal mycelium.[51] The biosynthesized AgNPs demonstrated promising antifungal activity against *A. niger*, *A. flavus*, and *F. oxysporum*, showcasing their potential in combating these fungal pathogens.[52] The synthesized AgNPs from the leaf extract of *Acalypha indica* showed effective antifungal properties against major phytopathogens, like *Alternaria alternata*, *Botrytis cinera*, and *Curvularia lunata*.[53] Green-synthesized AgNPs derived from Aloe vera plants demonstrated superior antifungal effects against *Aspergillus*. Microscopic observation revealed that these nanoparticles significantly hinder conidial germination and damage fungal hyphae, highlighting their potent antifungal capabilities.[54] Similarly, green-synthesized AgNPs were reported to exhibit remarkable antifungal activities against the five human pathogenic fungi *A. fumigatus*, *A. flavus*, *A. niger*, *Candida albicans*, and *Penicillium* sp., and three phytopathogenic fungi *F. oxysporum*, *R. solani*, and *Curvularia* sp.[55] Green-synthesized AgNPs from the root extract of *Diospyros paniculata* showed maximum antifungal activities against *A. flavus*, *P. notatum*, and *S. cerevisae* and a moderate effect against *A. niger* and *C. albicans*.[56] The mechanism and mode of action of AgNPs involve cell wall disintegration, surface proteins and nucleic acid damage by generating and accumulating reactive oxygen species, free radicals, and proton pump blockage.[57] Du *et al.* hypothesized that the accumulation of Ag$^+$ ions from AgNPs blocks respiration and that the efflux of intracellular ions leads to damage to the electron-transport system in the fungal cell.[58] Hence, these results confirmed that green-synthesized Hc-AgNPs could be an alternative growth inhibitor against various pathogenic microorganisms in agricultural and medical sectors, such as in preparing nano-eye drops. Fig. 11 show the remarkable inhibition efficiency of different concentrations of Hc-AgNPs against the fungi *F. oxysporum* and *A. flavus*.

3.9.   Antibacterial activity studies of the Hc-AgNPs

The antibacterial activity of Hc-AgNPs was studied against three Gram-negative phytopathogenic bacteria, namely *Xanthomonas oryzae*, *Ralstonia solanacearum*, and *Erwinia carotovora*, using the agar well diffusion method, as depicted in Fig. 12. Three different concentrations (168, 336, and 504 μg) of Hc-AgNPs were tested to determine the antibacterial effect, with ciprofloxacin used as the control. The results showed that the synthesized NPs had significant antibacterial potential against all the tested bacterial strains. The maximum zone of inhibition at the higher doses (504 μg) of Hc-AgNPs was found against *X. oryzae* as 16.33 ± 0.57 mm, whereas it was 15.33 ± 0.57 mm and 14.33 ± 0.57 mm against *R. solanacearum* and *E. carotovora*. When decreasing the concentration to 336 μg and 168 μg of NPs, the zones of inhibition were 13.66 ± 1.15 mm and 12 ± 1 mm against *X. oryzae*, 13.33 ± 0.57 mm and 10.33 ± 0.57 mm against *R. solanacearum*, and 12.33 ± 0.57 mm and 10.66 ± 0.57 mm against *E. carotovora*. On the other hand, ciproflaxin showed zones of inhibition of 33.66 ± 0.57, 31.66 ± 0.57, and

33.66 ± 0.57 mm against *X. oryzae*, *R. solanacearum*, and *E. carotovora*, respectively. The radial zone of inhibition was dose-dependent, as depicted in Table 4. The exact mechanism of action of AgNPs against bacteria is not entirely understood yet. However, several hypotheses are trying to uncover the mechanism of action of the antibacterial activity of AgNPs as: (1) the generation of free radicals leads to oxidative stress and ultimate cell death;[59,60] (2) the release of Ag$^+$ ions from AgNPs binds with sulphur- and phosphorus-containing compounds in the bacterial cell, such as DNA and proteins, which may block DNA replication, leading to a loss of cell viability and ultimately cell death;[60–62] (3) the release of Ag$^+$ ions inside the bacterial cell from AgNPs interact with the thiol group of NADH dehydrogenase enzymes, leading to disruption of the respiratory chain.[60,63] In the present study, synthesized Hc-AgNPs from *Hedychium coronarium* demonstrated a significant inhibition zone against all the tested bacterial strains. The corresponding average radial zone of inhibition for different bacteria at various concentrations of AgNPs is showcased effectively in Fig. 13. We performed a detailed comparison study of Hc-AgNPs with reported AgNPs in different applications in metal-ion sensing, and tested their antifungal and antibacterial activity, as shown in the ESI in Table S1.†

4.   Conclusion

This study successfully developed an environmentally friendly and commercially feasible method for producing stable silver nanoparticles (Hc-AgNPs) using leaf extract from *Hedychium coronarium*. Biosynthesis is considered a viable substitute because no additional capping agent is required to synthesize stable silver nanoparticles. *Hedychium coronarium* itself acts as an oxidizing as well as reducing agent for the conversion of Ag$^+$/Ag and produces stable Ag nanoparticles because of the presence of alkaloids, phenols, flavonoids, terpenoids, steroids, and glycosides in the *Hedychium coronarium* leaf extract. Hc-AgNPs were identified by searching for a surface plasmon resonance peak at 440 nm. These nanoparticles remained stable for six months without clumping or agglomerating. The Hc-AgNPs had an average crystallite size of 22.6 ± 1 nm at the (111) plane and a particle size of 22.42 ± 1 nm with a spherical shape. The Hc-AgNPs exhibited intriguing characteristics, like fluorescence with a peak emission at 504 nm and effective semiconducting behaviour with a bandgap energy of 3.78 eV. These characteristics could have a wide range of uses in electronic devices or sensors, depending on the characteristics of the nanoparticles. Hc-AgNPs were proven to be very selective for the colorimetric sensing of Sn^{2+} and Hg^{2+} compared to other metal ions. It demonstrated excellent antimicrobial properties against *Xanthomonas oryzae* bacterial strains (16.33 ± 0.57) compared to other Gram-negative bacteria. Outstanding antifungal activity was found in the Hc-AgNPs against *Aspergillus flavus* and *Fusarium oxysporum*. Therefore, these results validated the potential application of the green-synthesized Hc-AgNPs as an alternative growth inhibitor against a range of pathogenic microorganisms in the agricultural and medical domains, like nano eye drops for anti-allergic agents.

Data availability

The data supporting the findings of this article have been included as part of the ESI† and are available free of charge at DOI: https://doi.org/10.1039/D4NA00443D. The analytical characteristics of Hc-AgNPs data available at UV-visible spectroscopy (UV-1800, SHIMADZU) (Fig. 2, 7 and 8), FTIR (Fig. 3), powder X-ray diffraction (PANalytical X pert³) (Fig. 4), HR-TEM (HRTEM: Jeol/JEM 2100) (Fig. 5), fluorescence spectrophotometer (PerkinElmer FL 6500) (Fig. 6), antifungal (Fig. 10 and 11), and antimicrobial (Fig. 12 and 13) and Tables 3 and 4.

Author contributions

Under the guidance of Dr T. K. Ghorai and Dr A. K. Shukla, Mr S. K. Sahu, Mrs A. Kushwaha, Mr U. K. Pradhan and Mr P. Majhi carried out all of the experiments, characterization and applications. Mr S. K. Sahu write the manuscript and Dr T. K. Ghorai designed and corrected the whole manuscript.

Conflicts of interest

The authors declare no conflict of financial interest.

Acknowledgements

References

1 M. Annadhasan, T. Muthukumarasamyvel, V. R. Sankar Babu and N. Rajendiran, Green Synthesized Silver and Gold Nanoparticles for Colorimetric Detection of Hg2+, Pb2+, and Mn2+ in Aqueous Medium, *ACS Sustain. Chem. Eng.*, 2014, **2**, 887–896.

2 L. M. Liz-Marzán, Tailoring surface plasmons through the morphology and assembly of metal nanoparticles, *Langmuir*, 2006, **22**, 32–41.

3 K. L. Kelly, E. Coronado, L. L. Zhao and G. C. Schatz, The Optical Properties of Metal Nanoparticles: The Influence of Size, Shape, and Dielectric Environment, *J. Phys. Chem. B*, 2003, **107**, 668–677.

4 P. Liu and M. Zhao, Silver nanoparticle supported on halloysite nanotubes catalyzed reduction of 4-nitrophenol (4-NP), *Appl. Surf. Sci.*, 2009, **255**, 3989–3993.

5 P. D. Nallathamby, K. J. Lee and X.-H. N. Xu, Design of Stable and Uniform Single Nanoparticle Photonics for In Vivo Dynamics Imaging of Nanoenvironments of Zebrafish Embryonic Fluids, *ACS Nano*, 2008, **2**, 1371–1380.

6 R. Qu, W. Zhang, N. Liu, Q. Zhang, Y. Liu, X. Li, Y. Wei and L. Feng, Antioil Ag3PO4 Nanoparticle/Polydopamine/Al2O3 Sandwich Structure for Complex Wastewater Treatment: Dynamic Catalysis under Natural Light, *ACS Sustain. Chem. Eng.*, 2018, **6**, 8019–8028.

7 Y. Zhou, Y. Kong, S. Kundu, J. D. Cirillo and H. Liang, Antibacterial activities of gold and silver nanoparticles against Escherichia coli and bacillus Calmette-Guérin, *J. Nanobiotechnol.*, 2012, **10**, 1–9.

8 M. Zahran, M. El-Kemary, S. Khalifa and H. El-Seedi, Spectral studies of silver nanoparticles biosynthesized by Origanum majorana, *Green Process. Synth.*, 2018, **7**, 100–105.

9 R. Bhanumathi, M. Manivannan, R. Thangaraj and S. Kannan, Drug-Carrying Capacity and Anticancer Effect of the Folic Acid- and Berberine-Loaded Silver Nanomaterial To Regulate the AKT-ERK Pathway in Breast Cancer, *ACS Omega*, 2018, **3**, 8317–8328.

10 N. Tarannum, Divya and Y. K. Gautam, Facile green synthesis and applications of silver nanoparticles: A state-of-the-art review, *RSC Adv.*, 2019, **9**, 34926–34948.

11 S. K. Chandraker, M. Lal, P. Dhruve, R. P. Singh and R. Shukla, Cytotoxic, Antimitotic, DNA Binding, Photocatalytic, H2O2 Sensing, and Antioxidant Properties of Biofabricated Silver Nanoparticles Using Leaf Extract of Bryophyllum pinnatum (Lam.) Oken, *Front. Mol. Biosci.*, 2021, **7**, 593040.

12 S. K. Chandraker, M. Lal, F. Khanam, P. Dhruve, R. P. Singh and R. Shukla, Therapeutic potential of biogenic and optimized silver nanoparticles using Rubia cordifolia L. leaf extract, *Sci. Rep.*, 2022, **12**, 1–16.

13 S. K. Chandraker, M. Lal and R. Shukla, DNA-binding, antioxidant, H2O2 sensing and photocatalytic properties of biogenic silver nanoparticles using: Ageratum conyzoides L. leaf extract, *RSC Adv.*, 2019, **9**, 23408–23417.

14 S. Donga and S. Chanda, Facile green synthesis of silver nanoparticles using Mangifera indica seed aqueous extract and its antimicrobial, antioxidant and cytotoxic potential (3-in-1 system), *Artif. Cells, Nanomed., Biotechnol.*, 2021, **49**, 292–302.

15 I. I. Niyonshuti, V. R. Krishnamurthi, D. Okyere, L. Song, M. Benamara, X. Tong, Y. Wang and J. Chen, Polydopamine Surface Coating Synergizes the Antimicrobial Activity of Silver Nanoparticles, *ACS Appl. Mater. Interfaces*, 2020, **12**, 40067–40077.

16 A. P. C. Ribeiro, S. Anbu, E. C. B. A. Alegria, A. R. Fernandes, P. V Baptista, R. Mendes, A. S. Matias, M. Mendes, M. F. C. Guedes da Silva and A. J. L. Pombeiro, Evaluation of cell toxicity and DNA and protein binding of green synthesized silver nanoparticles, *Biomed. Pharmacother.*, 2018, **101**, 137–144.

17 Y. Rekik, V. Tardillo Suárez, V. R. Sharma, M. Chevallet, B. Gallet, D. Falconet, P. Charbonnier, I. Kieffer, R. Tucoulou, P. H. Jouneau, G. Veronesi and A. Deniaud, Deciphering silver nanoparticle fate in liver up to biliary excretion using HepG2/C3A spheroids in scenarios

mimicking different exposure pathways, *Environ. Sci.: Nano*, 2023, **10**, 1842–1857.

18 M. Shivakumar, K. L. Nagashree, S. Yallappa, S. Manjappa, K. S. Manjunath and M. S. Dharmaprakash, Biosynthesis of silver nanoparticles using pre-hydrolysis liquor of Eucalyptus wood and its effective antimicrobial activity, *Enzyme Microb. Technol.*, 2017, **97**, 55–62.

19 S. K. Chandraker, M. Lal, R. Shukla, M. K. Ghosh and T. K. Ghorai, Colorimetric sensing of Fe3+ and Hg2+ and photocatalytic activity of green synthesized silver nanoparticles from the leaf extract of: Sonchus arvensis L, *New J. Chem.*, 2019, **43**, 18175–18183.

20 S. Kassavetis, S. Kaziannis, N. Pliatsikas, A. Avgeropoulos, A. E. Karantzalis, C. Kosmidis, E. Lidorikis and P. Patsalas, Formation of plasmonic colloidal silver for flexible and printed electronics using laser ablation, *Appl. Surf. Sci.*, 2015, **336**, 262–266.

21 M. Darroudi, A. Khorsand Zak, M. R. Muhamad, N. M. Huang and M. Hakimi, Green synthesis of colloidal silver nanoparticles by sonochemical method, *Mater. Lett.*, 2012, **66**, 117–120.

22 L. Wang, J. Zhong, G. Li and J.-F. Chen, Preparation of silver nanopowders by a controlled wet-chemical synthesis, *Mater. Lett.*, 2016, **173**, 39–42.

23 Y. Wang, A. Chinnathambi, O. Nasif and S. A. Alharbi, Green synthesis and chemical characterization of a novel anti-human pancreatic cancer supplement by silver nanoparticles containing Zingiber officinale leaf aqueous extract, *Arabian J. Chem.*, 2021, **14**, 103081.

24 Y. He, X. Li, Y. Zheng, Z. Wang, Z. Ma, Q. Yang, B. Yao, Y. Zhao and H. Zhang, A green approach for synthesizing silver nanoparticles, and their antibacterial and cytotoxic activities, *New J. Chem.*, 2018, **42**, 2882–2888.

25 Z. Shervani and Y. Yamamoto, Carbohydrate-directed synthesis of silver and gold nanoparticles: effect of the structure of carbohydrates and reducing agents on the size and morphology of the composites, *Carbohydr. Res.*, 2011, **346**, 651–658.

26 H. Wei, Z. Wang, J. Zhang, S. House, Y.-G. Gao, L. Yang, H. Robinson, L. H. Tan, H. Xing, C. Hou, I. M. Robertson, J.-M. Zuo and Y. Lu, Time-dependent, protein-directed growth of gold nanoparticles within a single crystal of lysozyme, *Nat. Nanotechnol.*, 2011, **6**, 93–97.

27 S. Si and T. K. Mandal, Tryptophan-based peptides to synthesize gold and silver nanoparticles: A mechanistic and kinetic study, *Chem. - Eur. J.*, 2007, **13**, 3160–3168.

28 M. K. Ghosh, S. Sahu, I. Gupta and T. K. Ghorai, Green synthesis of copper nanoparticles from an extract ofJatropha curcasleaves: characterization, optical properties, CT-DNA binding and photocatalytic activity, *RSC Adv.*, 2020, **10**, 22027–22035.

29 K. Jadhav, S. Deore, D. Dhamecha, R. H R, S. Jagwani, S. Jalalpure and R. Bohara, Photosynthesis of Silver Nanoparticles: Characterization, Biocompatibility Studies, and Anticancer Activity, *ACS Biomater. Sci. Eng.*, 2018, **4**, 892–899.

30 M. S. Niloy, M. M. Hossain, M. Takikawa, M. S. Shakil, S. A. Polash, K. M. Mahmud, M. F. Uddin, M. Alam, R. D. Shubhra, M. M. A. K. Shawan, T. Saha, S. Takeoka, M. A. Hasan and S. Ranjan Sarker, Synthesis of Biogenic Silver Nanoparticles Using Caesalpinia digyna and Investigation of Their Antimicrobial Activity and in Vivo Biocompatibility, *ACS Appl. Bio Mater.*, 2020, **3**, 7722–7733.

31 M. Das and S. S. Smita, Biosynthesis of silver nanoparticles using bark extracts of Butea monosperma (Lam.) Taub. and study of their antimicrobial activity, *Appl. Nanosci.*, 2018, **8**, 1059–1067.

32 J. F. Al Mutairi, F. Al-Otibi, H. M. Alhajri, R. I. Alharbi, S. Alarifi and S. S. Alterary, Antimicrobial Activity of Green Silver Nanoparticles Synthesized by Different Extracts from the Leaves of Saudi Palm Tree (Phoenix Dactylifera L.), *Molecules*, 2022, **27**(10), 3113.

33 W. Huang, M. Yan, H. Duan, Y. Bi, X. Cheng and H. Yu, Synergistic Antifungal Activity of Green Synthesized Silver Nanoparticles and Epoxiconazole against Setosphaeria turcica, *J. Nanomater.*, 2020, 9535432.

34 G. Aragay, J. Pons and A. Merkoçi, Recent Trends in Macro-, Micro-, and Nanomaterial-Based Tools and Strategies for Heavy-Metal Detection, *Chem. Rev.*, 2011, **111**, 3433–3458.

35 E. M. Nolan and S. J. Lippard, Tools and Tactics for the Optical Detection of Mercuric Ion, *Chem. Rev.*, 2008, **108**, 3443–3480.

36 H. K. Sung, S. Y. Oh, C. Park and Y. Kim, Colorimetric Detection of Co2+ Ion Using Silver Nanoparticles with Spherical, Plate, and Rod Shapes, *Langmuir*, 2013, **29**, 8978–8982.

37 S. Ahmad Bhat, T. Hassan and S. Majid, Heavy metal toxicity and their harmful effects on living organisms- A Review, *Int. J. Med. Sci. Diagnosis Res.*, 2019, **3**, 106–122.

38 K. Kiran, Gold nanoparticles for mercury determination in environmental water and vegetable samples, *Appl. Nanosci.*, 2015, **5**, 361–366.

39 K. Farhadi, M. Forough, R. Molaei, S. Hajizadeh and A. Rafipour, Highly selective Hg2+ colorimetric sensor using green synthesized and unmodified silver nanoparticles, *Sens. Actuators, B*, 2012, **161**, 880–885.

40 S. Ali, M. R. Khan, M. Irfanullah, M. Sajid and Z. Zahra, Phytochemical investigation and antimicrobial appraisal of Parrotiopsis jacquemontiana (Decne) Rehder, *BMC Complement. Altern. Med.*, 2018, **18**, 43.

41 S. K. Chandraker, M. Lal, M. K. Ghosh, V. Tiwari, T. K. Ghorai and R. Shukla, Green synthesis of copper nanoparticles using leaf extract of Ageratum houstonianum Mill. and study of their photocatalytic and antibacterial activities, *Nano Express*, 2020, **1**, 010033.

42 Y. Rufai, Y. Isah and M. S. Isyaka, Comparative Phyto-Constituents Analysis from the Root Bark and Root Core Extractives of Cassia ferruginea (Schrad D. C) Plant, *Sch. J. Agric. Vet. Sci.*, 2016, **3**, 275–283.

43 R. Roghini and K. Vijayalakshmi, Phytochemical Screening, Quantitative Analysis of Flavonoids and Minerals in Ethanolic Extract of Citrus Paradisi, *Int. J. Pharma Sci. Res.*, 2018, **9**, 4859.

44 J. M. Ashraf, M. A. Ansari, H. M. Khan, M. A. Alzohairy and I. Choi, Green synthesis of silver nanoparticles and characterization of their inhibitory effects on AGEs formation using biophysical techniques, *Sci. Rep.*, 2016, **6**, 20414.

45 D. Garibo, H. A. Borbón-Nuñez, J. N. D. de León, E. García Mendoza, I. Estrada, Y. Toledano-Magaña, H. Tiznado, M. Ovalle-Marroquin, A. G. Soto-Ramos, A. Blanco, J. A. Rodríguez, O. A. Romo, L. A. Chávez-Almazán and A. Susarrey-Arce, Green synthesis of silver nanoparticles using Lysiloma acapulcensis exhibit high-antimicrobial activity, *Sci. Rep.*, 2020, **10**, 12805.

46 N. Satsangi, Synthesis and Characterization of Biocompatible Silver Nanoparticles for Anticancer Application, *J. Inorg. Organomet. Polym. Mater.*, 2020, **30**, 1907–1914.

47 M. R. Shaik, M. Khan, M. Kuniyil, A. Al-Warthan, H. Z. Alkhathlan, M. R. H. Siddiqui, J. P. Shaik, A. Ahamed, A. Mahmood, M. Khan and S. F. Adil, *Sustainability*, 2018, **10**.

48 S. Pirtarighat, M. Ghannadnia and S. Baghshahi, Green synthesis of silver nanoparticles using the plant extract of Salvia spinosa grown in vitro and their antibacterial activity assessment, *J. Nanostruct. Chem.*, 2019, **9**, 1–9.

49 D. Elumalai, M. Hemavathi, C. V. Deepaa and P. K. Kaleena, Evaluation of photosynthesised silver nanoparticles from leaf extracts of Leucas aspera and Hyptis suaveolens and their larvicidal activity against malaria, dengue and filariasis vectors, *Parasite Epidemiol. Control*, 2017, **2**, 15–26.

50 S. Kumar Chandraker, M. Kumar Ghosh, Parshant, A. Tiwari, T. Kumar Ghorai and R. Shukla, Efficient sensing of heavy metals (Hg2+ and Fe3+) and hydrogen peroxide from Bauhinia variegata L. fabricated silver nanoparticles, *Inorg. Chem. Commun.*, 2022, **146**, 110173.

51 M. Khan, A. U. Khan, N. Bogdanchikova and D. Garibo, *Molecules*, 2021, **26**(9), 2462.

52 D. H. Nguyen, J. S. Lee, K. D. Park, Y. C. Ching, X. T. Nguyen, V. H. G. Phan and T. T. Hoang Thi, *Nanomaterials*, 2020, **10**.

53 C. Krishnaraj, R. Ramachandran, K. Mohan and P. T. Kalaichelvan, Optimization for rapid synthesis of silver nanoparticles and its effect on phytopathogenic fungi, *Spectrochim. Acta, Part A*, 2012, **93**, 95–99.

54 S. Medda, A. Hajra, U. Dey, P. Bose and N. K. Mondal, Biosynthesis of silver nanoparticles from Aloe vera leaf extract and antifungal activity against Rhizopus sp. and Aspergillus sp, *Appl. Nanosci.*, 2015, **5**, 875–880.

55 P. Balashanmugam, M. D. Balakumaran, R. Murugan, K. Dhanapal and P. T. Kalaichelvan, Phytogenic synthesis of silver nanoparticles, optimization and evaluation of in vitro antifungal activity against human and plant pathogens, *Microbiol. Res.*, 2016, **192**, 52–64.

56 N. H. Rao, N. Lakshmidevi, S. V. N. Pammi, P. Kollu, S. Ganapaty and P. Lakshmi, Green synthesis of silver nanoparticles using methanolic root extracts of Diospyros paniculata and their antimicrobial activities, *Mater. Sci. Eng., C*, 2016, **62**, 553–557.

57 S. Mansoor, I. Zahoor, T. R. Baba, S. A. Padder, Z. A. Bhat, A. M. Koul and L. Jiang, Fabrication of Silver Nanoparticles Against Fungal Pathogens, *Frontal Nanotechnol. Res.*, 2021, **3**, 1–12.

58 H. Du, T.-M. Lo, J. Sitompul and M. W. Chang, Systems-level analysis of Escherichia coli response to silver nanoparticles: The roles of anaerobic respiration in microbial resistance, *Biochem. Biophys. Res. Commun.*, 2012, **424**, 657–662.

59 J. S. Kim, E. Kuk, K. N. Yu, J.-H. Kim, S. J. Park, H. J. Lee, S. H. Kim, Y. K. Park, Y. H. Park, C.-Y. Hwang, Y.-K. Kim, Y.-S. Lee, D. H. Jeong and M.-H. Cho, Antimicrobial effects of silver nanoparticles, *Nanomedicine*, 2007, **3**, 95–101.

60 K. Jyoti, M. Baunthiyal and A. Singh, Characterization of silver nanoparticles synthesized using Urtica dioica Linn. leaves and their synergistic effects with antibiotics, *J. Radiat. Res. Appl. Sci.*, 2016, **9**, 217–227.

61 Y. Matsumura, K. Yoshikata, S. ichi Kunisaki and T. Tsuchido, Mode of bactericidal action of silver zeolite and its comparison with that of silver nitrate, *Appl. Environ. Microbiol.*, 2003, **69**, 4278–4281.

62 K. Chaloupka, Y. Malam and A. M. Seifalian, Nanosilver as a new generation of nanoproduct in biomedical applications, *Trends Biotechnol.*, 2010, **28**, 580–588.

63 X. Wang, Y. Du, L. Fan, H. Liu and Y. Hu, Chitosan- metal complexes as antimicrobial agent: Synthesis, characterization and Structure-activity study, *Polym. Bull.*, 2005, **55**, 105–113.